Monitoring Meso-Scale Ordering of Cellulose in Intact Plant Cell Walls Using Sum Frequency Generation Spectroscopy[1][C][W][OPEN]

Yong Bum Park*, Christopher M. Lee, Bon-Wook Koo, Sunkyu Park, Daniel J. Cosgrove*, and Seong H. Kim*

Departments of Biology (Y.B.P., D.J.C.) and Chemical Engineering and Materials Research Institute (C.M.L., S.H.K.), Pennsylvania State University, University Park, Pennsylvania 16802; and Department of Forest Biomaterials, North Carolina State University, Raleigh, North Carolina 27695 (B.-W.K., S.P.)

ORCID ID: 0000-0001-8810-6077 (Y.B.P.).

Sum frequency generation (SFG) vibration spectroscopy can selectively detect crystalline cellulose without spectral interference from cell wall matrix components. Here, we show that the cellulose SFG spectrum is sensitive to cellulose microfibril alignment and packing within the cell wall. SFG intensity at 2,944 cm^{-1} correlated well with crystalline cellulose contents of various regions of the Arabidopsis (*Arabidopsis thaliana*) inflorescence, while changes in the 3,320/2,944 cm^{-1} intensity ratio suggest subtle changes in cellulose ordering as tissues mature. SFG analysis of two cellulose synthase mutants (*irx1/cesa8* and *irx3/cesa7*) indicates a reduction in cellulose content without evidence of altered cellulose structure. In primary cell walls of Arabidopsis, cellulose exhibited a characteristic SFG peak at 2,920 and 3,320 cm^{-1}, whereas in secondary cell walls, it had peaks at 2,944 and 3,320 cm^{-1}. Starch (amylose) gave an SFG peak at 2,904 cm^{-1} (CH methine) whose intensity increased with light exposure prior to harvest. Selective removal of matrix polysaccharides from primary cell walls by acid hydrolysis resulted in an SFG spectrum resembling that of secondary wall cellulose. Our results show that SFG spectroscopy is sensitive to the ordering of cellulose microfibrils in plant cell walls at the meso scale (nm to μm) that is important for cell wall architecture but cannot be probed by other spectroscopic or diffraction techniques.

Cellulose is a major component of lignocellulosic biomass as well as the most abundant biopolymer on Earth (Pauly and Keegstra, 2008). Chemically, cellulose is described as a linear polymer of 1→4-linked β-D-glucopyranose units. In plant cell walls, cellulose commonly exists in the form of approximately 3-nm-wide microfibrils containing numerous parallel glucan chains (variously estimated as 18–36) closely packed to form a highly ordered, or crystalline, structure (Doblin et al., 2002; Nishiyama et al., 2002; Somerville, 2006; Fernandes et al., 2011; Thomas et al., 2013). In primary cell walls, cellulose microfibrils are largely dispersed in a matrix of hemicelluloses and pectins, whereas in secondary walls, microfibrils are typically aggregated into larger bundles, approximately 10 to 20 nm in diameter, which are surrounded by hemicelluloses and lignin and highly aligned with each other (Kennedy et al., 2007; Fernandes et al., 2011). Native cellulose contains a combination of two crystalline allomorphs, I_α and I_β (Atalla and Vanderhart, 1984), as well as a large fraction of partially disordered chains at the surface of the microfibril and at noncrystalline segments of the microfibril that separate crystallites (Thomas et al., 2013). The structure of cellulose is important because of its fundamental role in plant mechanics, growth, and defense (Cosgrove, 2005) as well as in recalcitrance to enzymatic and chemical conversion to biofuel use (Pauly and Keegstra, 2008).

Cellulose in plant cell walls is hierarchically organized, spanning length scales from 10^{-9} to 10^{-2} m. At the nanometer scale, cellulose crystal structure is determined by how chains are packed and interact through intramolecular and intermolecular hydrogen bonds and van der Waals interactions. The distribution of disordered cellulose chains is an important structural feature, but it is difficult to assess (Thomas et al., 2013). At a larger scale, microfibrils are organized with hemicelluloses and other matrix polymers into a layer or series of layers that form a cohesive network encapsulating the whole cell, typically approximately 100 μm in length but up to many millimeters in the case of some fiber cells. Cellulose

[1] This work was supported by the U.S. Department of Energy, Office of Science, Office of Basic Energy Sciences (grant no. DE–SC0001090).

* Address correspondence to yzp107@psu.edu, dcosgrove@psu.edu, and shkim@engr.psu.edu.

The author responsible for distribution of materials integral to the findings presented in this article in accordance with the policy described in the Instructions for Authors (www.plantphysiol.org) is: Yong Bum Park (yzp107@psu.edu).

Y.B.P. designed and conducted overall experiments, and will take responsibility for every detail and request about how to prepare and analyze the plant cell wall samples. D.J.C. interpreted structural changes of cellulose of plant cell walls by development and mutations, and will take responsibility for data interpretation. S.H.K. will take responsibility and provide every detail about spectroscopic and diffraction measurements and analyses. Y.B.P., D.J.C., and S.H.K. wrote the paper. Y.B.P. had primary responsibility for final content.

[C] Some figures in this article are displayed in color online but in black and white in the print edition.

[W] The online version of this article contains Web-only data.

[OPEN] Articles can be viewed online without a subscription.

www.plantphysiol.org/cgi/doi/10.1104/pp.113.225235

microfibril alignment and bundling are important determinants of cell wall strength, mechanical anisotropy, and growth characteristics (Cosgrove and Jarvis, 2012) as well as enzymatic digestibility (Ding et al., 2012).

The crystalline structure and higher scale ordering of cellulose in plant cell walls is typically analyzed by x-ray diffraction (XRD) and solid-state ^{13}C-NMR as well as Raman and infrared (IR) spectroscopy (Park et al., 2009, 2010). While crystalline cellulose can generate diffraction peaks in XRD, diffuse scattering of x-rays by noncrystalline components of plant cell walls, such as hemicelluloses, lignin, and pectin, alters the baseline of the cellulose diffraction peaks that are inherently broad due to the small size of cellulose crystallites. This is particularly problematic for cellulose in primary cell walls and makes XRD analysis of cellulose structure in intact plant cell walls imprecise. Although XRD has been used widely to estimate cellulose crystallinity in secondary cell walls and lignocellulosic biomass, crystallinity measurements are inaccurate, as the value varies greatly with the data-fitting methods (Barnette et al., 2012). Likewise, spectral overlaps or interference from noncellulosic matrix polymers make it challenging to analyze cellulose structure in intact plant cell walls with ^{13}C-NMR and Raman and IR spectroscopy (Park et al., 2010).

Sum frequency generation (SFG) spectroscopy has the potential to selectively detect crystalline cellulose without spectral interference from other wall components (Barnette et al., 2011, 2012). SFG is a nonlinear optical process that occurs in crystalline materials with a noncentrosymmetric structure or at interfaces (Chen et al., 2002). These systems create a net polar ordering of certain molecular or functional groups. When such systems are irradiated with two high-intensity laser pulses of different frequencies, a new photon can be emitted whose frequency is the sum of the two input frequencies (Shen, 1989). If one of the incident photons is in resonance with the vibration modes of the functional groups arranged with the net polar ordering within coherence length of the measurement, then vibration spectra of those modes can be obtained without interference from other modes that do not meet the noncentrosymmetry requirement. Since the glucan chains in cellulose I point in the same direction, the CH_2 groups of carbon 6 (hereafter $C6H_2$) and the O3H-O5 groups can form net dipoles across the entire crystallite or across multiple closely packed crystallites, resulting in characteristic SFG peaks at 2,944 cm^{-1} due to CH_2 vibration modes and at 3,320 to 3,350 cm^{-1} due to OH vibration modes (Lee et al., 2013a, 2013b). Other vibration modes in the cellulose crystal whose dipole moments cancel one another are SFG inactive. The same is true for hemicellulose and lignin, because these molecules are largely disordered in the cell wall and, consequently, do not generate SFG signals. Similarly, water molecules absorbed to cellulose and matrix polymers in the wall do not generate SFG peaks because they are not highly ordered. SFG spectroscopy has been applied to isolated celluloses and wood chips (Barnette et al., 2011, 2012) as well as cotton (*Gossypium hirsutum*) fibers (Hieu et al., 2011), but its potential for investigating changes in native cellulose order during plant development has not been assessed. The coherence length of SFG is estimated as a few hundred nanometers (Lacomb et al., 2008). Thus, SFG can reveal polar ordering of cellulose microfibril organization in the meso-scale, bridging structural information between the molecular scale less than or equal to nanometers and the macro scale larger than micrometers.

In this work, we used SFG spectroscopy in combination with other methods to detect changes in the ordering (or packing) of cellulose microfibrils in Arabidopsis (*Arabidopsis thaliana*), an important model plant for cell wall study (Chen et al., 1998; Liepman et al., 2010). The results reveal subtle changes in cellulose ordering and packing that are difficult to detect by common analytic methods.

RESULTS AND DISCUSSION

Monitoring Secondary Wall Cellulose during Inflorescence Formation

The elongating inflorescence of 6-week-old Arabidopsis plants presents a developmental gradient: older cells with thickened secondary cell walls are located at the base of the inflorescence, and younger cells with predominantly primary cell walls are at the top (Supplemental Fig. S1; Zhong et al., 2008). To assess potential changes in cellulose ordering along this gradient, we prepared cell wall pellets from five equally spaced regions along the inflorescence and analyzed them by SFG. For inflorescences of 6-week-old plants (6WAI), we observed a large change in the strength of the 2,944 cm^{-1} peak, with the highest intensity in the basal region and progressively weaker signals in higher (younger) regions of the inflorescence (Fig. 1A). In contrast, the 2,944 cm^{-1} peak was nearly the same along the inflorescences of 8-week-old plants (8WAI; Fig. 1B), where cell elongation had ceased and secondary walls were well developed at the top and bottom of the inflorescence. There was a good correlation between crystalline cellulose contents estimated by the method of Updegraff (1969) and by the 2,944 cm^{-1} intensity matched to a cellulose calibration curve (Fig. 1C; Supplemental Table S1; Barnette et al., 2012).

We also used a modified procedure in which SFG spectra were collected from short (approximately 10-mm) segments of inflorescence stem split open to collect spectra primarily from the internal stele and pith tissues. The results were qualitatively the same as those obtained with pellets and furthermore did not require decolorizing in ethanol (Supplemental Fig. S1, B–D), showing the potential of SFG for rapid and simple assessment of cellulose in complex tissues. Independent confirmation of these results was obtained by XRD analysis (Supplemental Fig. S2) and Raman spectra (Supplemental Fig. S3), whereas IR spectra proved uninformative (Supplemental Fig. S4). These results demonstrate SFG spectroscopy to be an effective means for

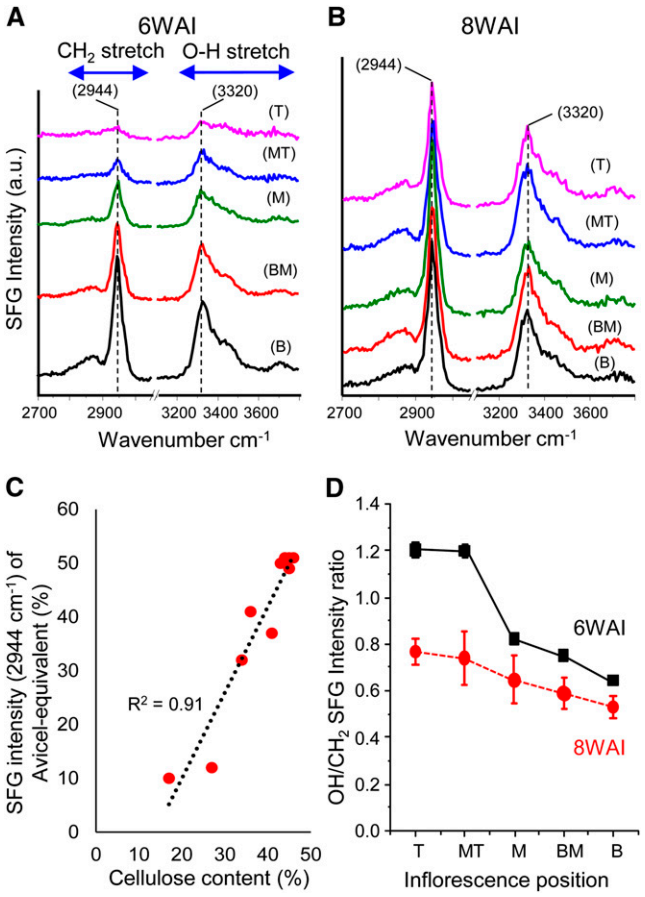

Figure 1. SFG spectra of ground wall pellets from different axial locations of stems from 6WAI (A) and 8WAI (B) of wild-type (Col-0) plants. Inflorescence stem regions are as follows: B, bottom (5%–20%); BM, bottom-middle (20%–40%); M, middle (40%–60%); MT, middle-top (60%–80%); T, top (80%–95%). C, Correlations of SFG intensity of the 2,944 cm^{-1} peak with crystalline cellulose values of 6WAI and 8WAI (r^2 = 0.91; n = 5 for SFG, n = 3 for 6WAI and 8WAI crystalline content). D, OH (3,320 cm^{-1})/CH_2 (2,944 cm^{-1}) SFG intensity ratio of 6WAI and 8WAI of the wild type (Col-0). Error bars represent SE ($8 \leq n \leq 10$). Some error bars are not seen because they are too small. SFG experiments (A and B) were repeated three times with similar results. a.u., Arbitrary unit. [See online article for color version of this figure.]

estimating the crystalline cellulose contents of plant cell walls without extraction of matrix wall polymers.

In addition to the good correlation between SFG intensity and cellulose contents, we noted changes in the 3,320/2,944 cm^{-1} intensity ratio along the inflorescence, with larger changes in 6WAI compared with 8WAI (Fig. 1D). This variation suggests that the relative polar ordering of the $C6H_2$ group (2,944 cm^{-1}) and the intrachain hydrogen-bonded O3H-O5 group (3,320 cm^{-1}) changes as the walls mature, dehydrate, or accumulate thicker secondary cell walls. In secondary cell walls, microfibrils are more aligned and closely packed compared with primary cell walls (Fernandes et al., 2011). The effects of lateral packing or distance between cellulose microfibrils might exert different effects on optical coherence of the $C6H_2$ and O3H-O5 groups. Another possible factor affecting the $C6H_2$ SFG intensity could be the twisting of cellulose microfibrils (Hanley et al., 1997), which likely reduces the net polar ordering of the $C6H_2$ group along the cellulose chain; in contrast, the SFG signal from the O3H-O5 group, which runs parallel with the microfibril axis, might not be affected by such twisting. Microfibrils of primary cell walls, which are relatively dispersed and unbundled, may be more subject to twisting than well-aligned and bundled microfibrils (Fernandes et al., 2011). Thus, the variation of the 3,320/2,944 cm^{-1} intensity ratio along the growth rate of the inflorescence may indicate such aspects of cellulose ordering that are currently difficult to assess with other methods. This suggests that, in addition to $C6H_2$ SFG intensity, the OH/$C6H_2$ intensity ratio can be used as a new indicator to advance our understanding of cellulose structure in intact plant walls.

Cellulose Alterations in Synthase Mutants

Ten putative cellulose synthase (*CesA*) genes have been identified in Arabidopsis (Richmond, 2000); among them, *CesA4*, *CesA7*, and *CesA8* contribute to cellulose synthesis in secondary cell walls (Turner and Somerville, 1997; Taylor et al., 2003). *CesA* defects often reduce cellulose

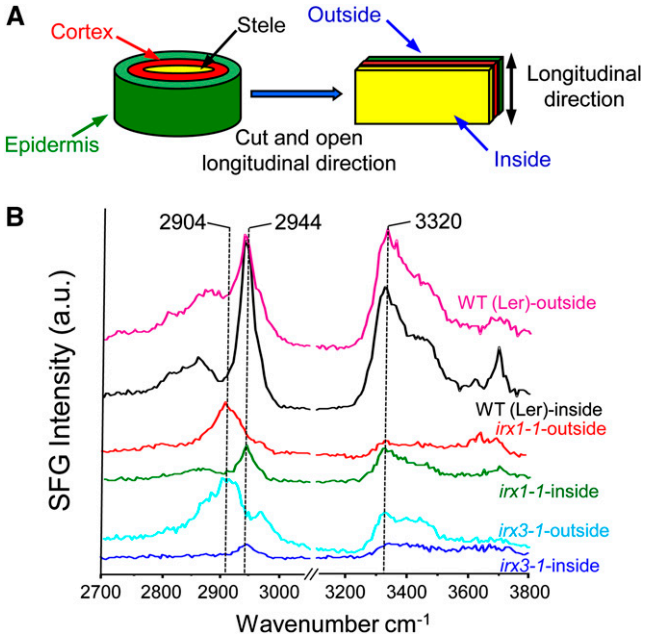

Figure 2. SFG measurements of the inside and outside from 8-week-old wild-type (WT) Landsberg *erecta* (Ler), *irx1-1*, and *irx3-1* inflorescences. A, Diagram of an intact Arabidopsis inflorescence sample for SFG analysis. Inside (stele) and outside (epidermis) tissues were exposed to IR and Raman spectroscopy for SFG measurement as illustrated. B, The inflorescence stems were cut in the middle region (see "Materials and Methods"). SFG measurements were repeated three times with similar results. a.u., Arbitrary unit. [See online article for color version of this figure.]

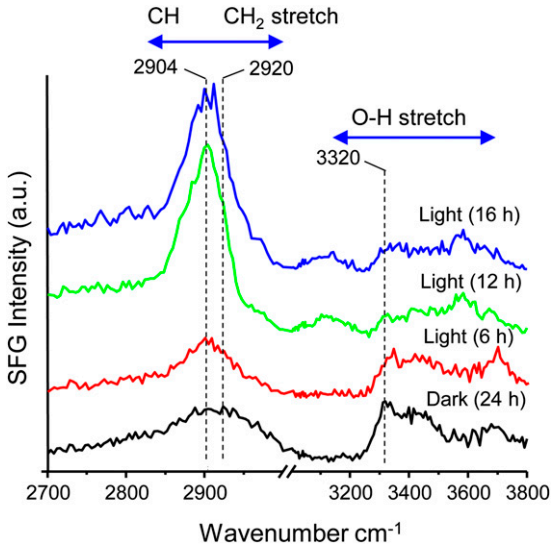

Figure 3. SFG spectra of 4WAA (Col-0) aerial tissue (pellets). Prior to harvesting, 4WAA was additionally grown for the indicated times under the dark or light. a.u., Arbitrary unit. [See online article for color version of this figure.]

contents, evidenced by XRD, histochemistry, and Updegraff assays, and result in small, weak plants (Turner and Somerville, 1997; Taylor et al., 2000; Wu et al., 2000; Zhong et al., 2008; Harris et al., 2012). To assess whether such mutations also modified other features of cellulose organization, we examined two *CesA* mutants, *CesA8*$^{irx1\text{-}1}$ (*irx1-1*) and *CesA7*$^{irx3\text{-}1}$ (*irx3-1*; Taylor et al., 2003), using bisected inflorescence stems as well as compressed pellets for SFG analysis. With the bisected stems, we collected SFG spectra at both the outside and inside of the stem. Figure 2 shows representative SFG spectra. Walls from the wild type showed prominent SFG peaks at 2,944 and 3,320 cm^{-1} for spectra collected from both the inside and outside surfaces. The relatively strong intensity of the 2,944 cm^{-1} peak for the inside surface is consistent with the prominence of secondary walls at or close to this surface. The reduced intensity of the 2,944 cm^{-1} peak for the outside wall spectra is likely due to the attenuation of the incident laser pulse in the epidermis, which contains mostly primary cells with relatively weak SFG contribution.

In comparison with the wild type, the SFG spectra obtained with the two *CesA* mutants were weaker, especially for the inside samples. Also, independent confirmation of the reduction of cellulose contents in *irx1-1* and *irx3-1* was obtained by XRD and Raman measurements (Supplemental Fig. S5). These result are consistent with the reduced cellulose contents in vascular walls reported for these mutants (Turner and Somerville, 1997). Taylor et al. (2000) reported that the xylem walls of *irx1* and *irx3* were indistinguishable at the microscopic level compared with the wild type, despite reduced cellulose contents. This is consistent with our SFG results, which did not show evidence of changes in cellulose ordering in the same *CesA* mutants. A second notable difference from the wild type was a weak but dominant peak at 2,904 cm^{-1} for spectra collected at the outside surface. The 2,904 cm^{-1} SFG peak is a characteristic CH (methine) signal of starch (amylose; Snyder et al., 1984; Miyauchi et al., 2006). When the cellulose signal was strong, the starch SFG signal was not prominent. However, when the cellulose signal was weak, then the starch signal could become dominant. Thus, it should be noted that starch signal can be a main CH SFG peak when

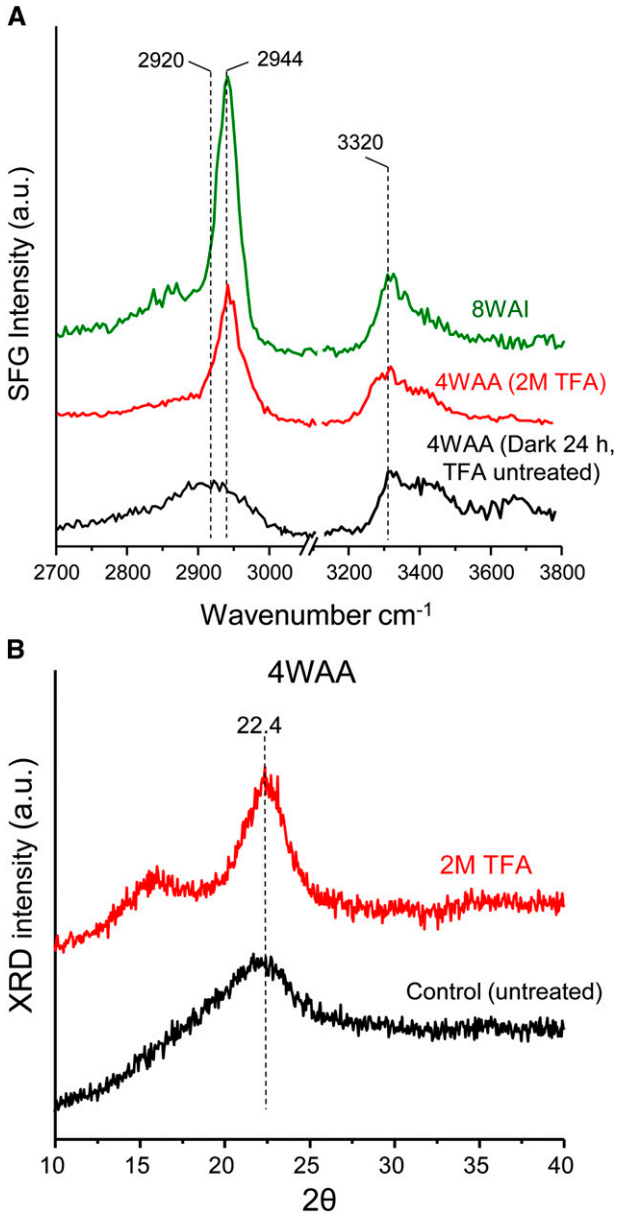

Figure 4. SFG and XRD measurements of Arabidopsis (Col-0) walls. A, Changes of SFG spectra of 4WAA (Col-0) aerial tissue (pellets) by 2 M TFA treatment. B, Increase of XRD crystal size of 4WAA after 2 M TFA treatment. a.u., Arbitrary unit. [See online article for color version of this figure.]

crystalline cellulose contents are greatly reduced by mutations.

SFG Spectral Differences between Cellulose of Primary and Secondary Cell Walls

Pulverized samples consisting predominantly of primary cell walls of aerial tissues of 4-week-old Arabidopsis (4WAA) were decolorized in ethanol and pressed into pellets for spectral analysis (Fig. 3). In contrast to the SFG spectra of cellulose microfibrils in secondary cell walls (Fig. 1), SFG signals of primary cell walls of 4WAA were notably weak and different. They exhibited a broad peak centered at 2,904 cm^{-1} and a very weak peak at 3,320 cm^{-1} (Fig. 3). The strong peak at 2,904 cm^{-1} is due to starch (amylose) contaminant in the primary cell wall sample. In order to deplete starch, plants were placed in darkness for 24 h prior to harvest (Zablackis et al., 1995; Graf et al., 2010). With the reduction in starch content, the SFG spectra of the primary cell walls could be assessed more clearly. The peak shape and position in the OH region were the same as the secondary cell wall SFG spectra, but the peak in the CH_2 stretch region was broad and centered at approximately 2,920 cm^{-1} instead of 2,944 cm^{-1}. The markedly distinct spectra for primary and secondary walls indicate that the SFG spectrum of cellulose is not determined solely by cellulose crystallite structure but may also be sensitive to the packing, twisting, and order of cellulose microfibrils, which differ for primary and secondary cell walls.

Additional support for this interpretation comes from an analysis of primary cell wall samples (4WAA) treated with 2 M trifluoroacetic acid (TFA), which hydrolyzes noncrystalline polysaccharides but does not alter crystalline cellulose structure (Vignon et al., 2004; Foster et al., 2010). The point of the TFA hydrolysis experiment was to test the idea that changes in the meso-scale ordering/alignment of cellulose microfibrils result in altered SFG spectra. SFG signal intensities increased after TFA hydrolysis and the spectrum changed markedly, giving peaks at 2,944 and 3,320 cm^{-1} (Fig. 4A; i.e. closely resembling spectra of celluloses in secondary cell walls). The increase in SFG intensities could be attributed to the increase in cellulose concentration upon the removal of matrix polymers (Barnette et al., 2012). However, without structural changes of crystalline cellulose, the SFG peak positions will not change. The appearance of the 2,944 and 3,320 cm^{-1} peaks after hydrolysis with 2 M TFA implied the conversion or alteration of cellulose microfibril spacing, alignment, and packing into a state similar to the secondary cell walls. The TFA treatment does not hydrolyze the crystalline cellulose and is unlikely to alter cellulose crystal structure. Thus, the observed changes in the SFG spectra must be due to changes in the optical coherence of net dipoles spaced over multiple cellulose crystals. Such coherence and microfibrillar packing are evidently different in the 4WAA primary cell walls, which lack the 2,944 cm^{-1} peak, but can be artificially created when matrix polymers are removed and the crystalline cellulose microfibrils collapse upon each other. In XRD, 4WAA treated with 2 M TFA revealed a larger crystal size than the untreated control (Fig. 4B). This process may be related to the induction of lateral association of microfibrils visualized in onion (*Allium cepa*) parenchyma walls after extraction to remove pectins and hemicelluloses (McCann et al., 1990).

To conclude, we found distinctive SFG spectra for cellulose in primary and secondary cell walls of various Arabidopsis tissues; additionally, after acid hydrolysis of noncrystalline polysaccharides, the SFG spectrum of primary cell walls changed to one resembling secondary cell walls. Our results indicate that SFG spectra are sensitive to the ordering (i.e. alignment, packing) of cellulose microfibrils in the cell wall. Such ordering is important for various physical properties of the wall, including tensile strength, compression resistance, and enzymatic digestibility of secondary walls, and for the ability to resist turgor pressure and to expand in primary cell walls.

MATERIALS AND METHODS

Plant Cell Wall Materials

After 4 d of cold treatment at 4°C, Arabidopsis (*Arabidopsis thaliana*) wild-type plants (Columbia [Col-0] and Landsberg *erecta*) and genetic mutants were grown on 1× or 0.5× Murashige and Skoog medium (Murashige and Skoog, 1962) containing 1% (w/v) Suc for 1 week, transferred onto soil, and grown under 70 μmol m^{-2} s^{-1} light intensity (day/night, 16/8 h; temperature, 22°C/16°C). Cell wall samples were collected from 4WAA aerial tissues, consisting of leaves and petioles. Unless otherwise stated, all Arabidopsis plants were exposed to light at least for 8 h or as indicated prior to harvest. The collected sample was frozen at –80°C, incubated in 100% (v/v) ethanol (with two exchanges of ethanol) at room temperature for 24 h to remove chlorophylls, rinsed with deionized distilled water, ground with mortar and pestle in liquid nitrogen, lyophilized, and pressed into pellets for SFG measurement. To remove noncrystalline cell wall components, the alcohol-insoluble residue (approximately 5 mg) was treated with 2 M TFA at 121°C for 90 min.

The main inflorescence stems were collected, frozen at –80°C, incubated in 100% ethanol (with two exchanges of ethanol) at room temperature for 24 h to remove chlorophylls, rinsed briefly with ddH_2O (deionized distilled water), frozen in liquid nitrogen, pulverized with mortar and pestle, lyophilized, and finally pressed into pellets at 650 bar for SFG, XRD, and Raman measurements. In some cases, the inflorescence stems were cut into five regions: bottom, 5% to 20%; bottom-middle, 20% to 40%; middle, 40% to 60%; middle-top, 60% to 80%; and top, 80% to 95%, where % is the height from the bottom/total plant. For cell wall histochemistry and wall component analysis, see Supplemental Materials and Methods S1.

SFG Spectroscopy Measurements

SFG signals were generated using an EKSPLA PL2241 picosecond mode-locked Nd:YAG laser, as described previously (Barnette et al., 2011; Lee et al., 2013a). The IR (parallel [p]-polarized, 300–350 μJ) and visible (senkrecht or perpendicular [s]-polarized, 41–200 μJ) beams were overlapped spatially and temporally on the sample with reflection geometry. The incidence angles of IR and visible laser beams were 56° and 60°, respectively, with respect to the surface normal. The SFG signal from the sample was collected with a beam collimator, filtered with an MS2011 monochromator (s-polarized), and detected with a photomultiplier (Hamamatsu). SFG spectra were obtained with an 8 cm^{-1} per step scan in the O-H stretching region (3,000–3,800 cm^{-1}) and a 4 cm^{-1} per step scan in the C-H stretching region (2,700–3,000 cm^{-1}) under ambient conditions. At each wave number, the detected SFG intensity was averaged over 100 laser shots and normalized over the visible and IR input beam intensities. In each SFG spectrum, the square of the effective nonlinear susceptibility is plotted as a function of input IR frequency in units of cm^{-1}. The SFG probe size was approximately 190 ± 10 μm along the laser incidence plane direction,

approximately 150 ± 10 μm perpendicular to the incident plane, and approximately 20 ± 5 μm in depth from the external surface of the sample.

Additional steps were needed to acquire SFG spectra from 6WAI and 8WAI pellets. To deal with texture variations of the samples, average SFG intensities at 2,944 and 3,320 cm^{-1} were first taken from four to six locations on the pellet. Complete SFG spectra were taken at locations on the pellet where the SFG signal was equal to the average intensity obtained from these four to six locations. Sample damage due to high-power laser pulses did not occur at the lowest visible power (approximately 41 μJ) needed to get sufficient signal-to-noise ratios. To verify this, the SFG signal was monitored at 2,944 cm^{-1} for 15 min to confirm no decrease in intensity over this time period. All intact samples were analyzed with the plane of incidence parallel with the longitudinal direction of the inflorescence and repeated three times for 6WAI and 8WAI (Supplemental Fig. S1). For IR and Raman measurements, see Supplemental Materials and Methods S1.

XRD Measurements

XRD analysis was performed using a Rigaku SmartLab XRD apparatus with a Cu tube (λ = 1.5405 Å). The radiation was generated at 25 mA and 35 kV. The scattering angle of 2θ (x-ray diffraction angle in degrees) from 9° to 41° was measured at the step size of 0.05° with 5-s exposure at each step. The pelletized sample was placed on a sample holder to ensure a flat, even surface. The crystallinity index was calculated using the amorphous subtraction method (Park et al., 2010). A mixture of xylan and lignin was used as an amorphous standard, and its portion was subtracted from the sample XRD spectrum. A scale factor was applied to the amorphous standard spectrum, so that the baseline between the crystalline XRD peaks is zero without any negative values after subtraction of the amorphous portion.

Supplemental Data

The following materials are available in the online version of this article.

Supplemental Figure S1. SFG spectra and toluidine blue staining of 6WA and 8WAI.

Supplemental Figure S2. XRD of 6WAI and 8WAI.

Supplemental Figure S3. Raman spectra of 6WAI and 8WAI.

Supplemental Figure S4. IR spectra of 6WAI and 8WAI.

Supplemental Figure S5. XRD and Raman spectra of 8WAI of wild type, *irx1-1*, and *irx3-1*.

Supplemental Table S1. Cell wall compositions of 6WAI and 8WAI.

Supplemental Materials and Methods S1. Cell wall histochemistry and wall component analysis, and IR and Raman measurements.

ACKNOWLEDGMENTS

We thank Mr. Edward Wagner and Ms. Liza Wilson for technical assistance for toluidine blue staining and Raman measurements.

Received July 19, 2013; accepted August 28, 2013; published August 30, 2013.

LITERATURE CITED

Atalla RH, Vanderhart DL (1984) Native cellulose: a composite of two distinct crystalline forms. Science **223:** 283–285

Barnette AL, Bradley LC, Veres BD, Schreiner EP, Park YB, Park J, Park S, Kim SH (2011) Selective detection of crystalline cellulose in plant cell walls with sum-frequency-generation (SFG) vibration spectroscopy. Biomacromolecules **12:** 2434–2439

Barnette AL, Lee CM, Bradley LC, Schreiner EP, Park YB, Shin H, Cosgrove DJ, Park S, Kim SH (2012) Quantification of crystalline cellulose in lignocellulosic biomass using sum frequency generation (SFG) vibration spectroscopy and comparison with other analytical methods. Carbohydr Polym **89:** 802–809

Chen L, Carpita NC, Reiter WD, Wilson RH, Jeffries C, McCann MC (1998) A rapid method to screen for cell-wall mutants using discriminant analysis of Fourier transform infrared spectra. Plant J **16:** 385–392

Chen Z, Shen YR, Somorjai GA (2002) Studies of polymer surfaces by sum frequency generation vibrational spectroscopy. Annu Rev Phys Chem **53:** 437–465

Cosgrove DJ (2005) Growth of the plant cell wall. Nat Rev Mol Cell Biol **6:** 850–861

Cosgrove DJ, Jarvis MC (2012) Comparative structure and biomechanics of plant primary and secondary cell walls. Front Plant Sci **3:** 204

Ding SY, Liu YS, Zeng Y, Himmel ME, Baker JO, Bayer EA (2012) How does plant cell wall nanoscale architecture correlate with enzymatic digestibility? Science **338:** 1055–1060

Doblin MS, Kurek I, Jacob-Wilk D, Delmer DP (2002) Cellulose biosynthesis in plants: from genes to rosettes. Plant Cell Physiol **43:** 1407–1420

Fernandes AN, Thomas LH, Altaner CM, Callow P, Forsyth VT, Apperley DC, Kennedy CJ, Jarvis MC (2011) Nanostructure of cellulose microfibrils in spruce wood. Proc Natl Acad Sci USA **108:** E1195–E1203

Foster CE, Martin TM, Pauly M (2010) Comprehensive compositional analysis of plant cell walls (lignocellulosic biomass) part II: carbohydrates. J Vis Exp **37:** doi/10.3791/1745

Graf A, Schlereth A, Stitt M, Smith AM (2010) Circadian control of carbohydrate availability for growth in Arabidopsis plants at night. Proc Natl Acad Sci USA **107:** 9458–9463

Hanley SJ, Revol J-F, Godbout L, Gray DG (1997) Atomic force microscopy and transmission electron microscopy of cellulose from *Micrasterias denticulata*; evidence for a chiral helical microfibril twist. Cellulose **4:** 209–220

Harris DM, Corbin K, Wang T, Gutierrez R, Bertolo AL, Petti C, Smilgies DM, Estevez JM, Bonetta D, Urbanowicz BR, et al (2012) Cellulose microfibril crystallinity is reduced by mutating C-terminal transmembrane region residues CESA1A903V and CESA3T942I of cellulose synthase. Proc Natl Acad Sci USA **109:** 4098–4103

Hieu HC, Tuan NA, Li H, Miyauchi Y, Mizutani G (2011) Sum frequency generation microscopy study of cellulose fibers. Appl Spectrosc **65:** 1254–1259

Kennedy CJ, Cameron GJ, Sturcova A, Apperley DC, Altaner C, Wess TJ, Jarvis MC (2007) Microfibril diameter in celery collenchyma cellulose: x-ray scattering and NMR evidence. Cellulose **14:** 235–246

Lacomb R, Nadiarnykh O, Townsend SS, Campagnola PJ (2008) Phase matching considerations in second harmonic generation from tissues: effects on emission directionality, conversion efficiency and observed morphology. Opt Commun **281:** 1823–1832

Lee CM, Mittal A, Barnette AL, Kafle K, Park YB, Shin H, Johnson DK, Park S, Kim SH (2013a) Cellulose polymorphism study with sum-frequency-generation (SFG) vibration spectroscopy: identification of exocyclic CH_2OH conformation and chain orientation. Cellulose **20:** 991–1000

Lee CM, Mohamed NM, Watts HD, Kubicki JD, Kim SH (2013b) Sum-frequency-generation vibration spectroscopy and density functional theory calculations with dispersion corrections (DFT-D2) for cellulose Iα and Iβ. J Phys Chem B **117:** 6681–6692

Liepman AH, Wightman R, Geshi N, Turner SR, Scheller HV (2010) Arabidopsis: a powerful model system for plant cell wall research. Plant J **61:** 1107–1121

McCann MC, Wells B, Roberts K (1990) Direct visualization of cross-links in the primary cell wall. J Cell Sci **96:** 323–334

Miyauchi Y, Sano H, Mirzutani G (2006) Selective observation of starch in a water plant using optical sum-frequency microscopy. J Opt Soc Am A Opt Image Sci Vis **23:** 1687–1690

Murashige T, Skoog F (1962) A revised medium for rapid growth and bioassays with tobacco tissue culture. Physiol Plant **15:** 473–497

Nishiyama Y, Langan P, Chanzy H (2002) Crystal structure and hydrogen-bonding system in cellulose Ibeta from synchrotron x-ray and neutron fiber diffraction. J Am Chem Soc **124:** 9074–9082

Park S, Baker JO, Himmel ME, Parilla PA, Johnson DK (2010) Cellulose crystallinity index: measurement techniques and their impact on interpreting cellulase performance. Biotechnol Biofuels **3:** 1–10

Park S, Johnson DK, Ishizawa CI, Parilla PA, Davis MF (2009) Measuring the crystallinity index of cellulose by solid state ^{13}C nuclear magnetic resonance. Cellulose **16:** 641–647

Pauly M, Keegstra K (2008) Cell-wall carbohydrates and their modification as a resource for biofuels. Plant J **54:** 559–568

Richmond T (2000) Higher plant cellulose synthases. Genome Biol **1:** reviews3001.3001–reviews3001.3006

Shen YR (1989) Surface properties probed by second-harmonic and sum-frequency generation. Nature **337:** 519–525

Snyder RG, Aljibury AL, Strauss HL, Casal HL, Gough KM, Murphy WJ (1984) Isolated C-H stretching vibrations of N-alkanes: assignments and relation to structure. J Chem Phys **81:** 5352–5361

Somerville C (2006) Cellulose synthesis in higher plants. Annu Rev Cell Dev Biol **22:** 53–78

Taylor NG, Howells RM, Huttly AK, Vickers K, Turner SR (2003) Interactions among three distinct CesA proteins essential for cellulose synthesis. Proc Natl Acad Sci USA **100:** 1450–1455

Taylor NG, Laurie S, Turner SR (2000) Multiple cellulose synthase catalytic subunits are required for cellulose synthesis in *Arabidopsis*. Plant Cell **12:** 2529–2540

Thomas LH, Forsyth VT, Sturcová A, Kennedy CJ, May RP, Altaner CM, Apperley DC, Wess TJ, Jarvis MC (2013) Structure of cellulose microfibrils in primary cell walls from collenchyma. Plant Physiol **161:** 465–476

Turner SR, Somerville CR (1997) Collapsed xylem phenotype of *Arabidopsis* identifies mutants deficient in cellulose deposition in the secondary cell wall. Plant Cell **9:** 689–701

Updegraff DM (1969) Semimicro determination of cellulose in biological materials. Anal Biochem **32:** 420–424

Vignon MR, Heux L, Malainine ME, Mahrouz M (2004) Arabinan-cellulose composite in Opuntia ficus-indica prickly pear spines. Carbohydr Res **339:** 123–131

Wu L, Joshi CP, Chiang VL (2000) A xylem-specific cellulose synthase gene from aspen (*Populus tremuloides*) is responsive to mechanical stress. Plant J **22:** 495–502

Zablackis E, Huang J, Müller B, Darvill AG, Albersheim P (1995) Characterization of the cell-wall polysaccharides of *Arabidopsis thaliana* leaves. Plant Physiol **107:** 1129–1138

Zhong R, Lee C, Zhou J, McCarthy RL, Ye ZH (2008) A battery of transcription factors involved in the regulation of secondary cell wall biosynthesis in *Arabidopsis*. Plant Cell **20:** 2763–2782